Hotspot DAXX, PTCH2 and CYFIP2 mutations in pancreatic neuroendocrine neoplasms

Accepted Preprint first posted on 18 July 2018 as Manuscript ERC-18-0120

Hotspot *DAXX, PTCH2* and *CYFIP2* mutations in pancreatic neuroendocrine neoplasms

Vandamme T[1,2,*], Beyens M[1,*], Boons G[1], Schepers A[3], Kamp K[2], Biermann K[4], Pauwels P[5], De Herder W.W.[2], Hofland L.J.[2], Peeters M[1], Van Camp G[3], Op de Beeck K[1]

1. Department of Oncology, University of Antwerp, Universiteitsplein 1, 2610 Antwerp, Belgium

2. Section of Endocrinology, Department of Internal Medicine, Section of Endocrinology, Erasmus Medical Center, Dr. Molenwaterplein 50, 3015GE Rotterdam, The Netherlands

3. Center of Medical Genetics, University of Antwerp, Universiteitsplein 1, 2610 Antwerp, Belgium

4. Department of Pathology, Erasmus Medical Center, Dr. Molenwaterplein 50, 3015GE Rotterdam, The Netherlands

5. Department of Pathology, University of Antwerp, Universiteitsplein 1, 2610 Antwerp, Belgium

** Equal contributing authors*

Short title: Recurrent DAXX, PTCH2 and CYFIP mutations in pNEN

Key words: Neuroendocrine tumors, Molecular genetics, Ultra-deep sequencing, Pancreatic neuroendocrine tumors, DAXX

Word count: 4602

Corresponding author: Timon Vandamme, Department of Oncology, University of Antwerp, Universiteitsplein 1, 2610 Wilrijk, Belgium. Telephone: +32 3 275 97 81, Fax: ,+32 3 275 97 23, e-mail: timon.vandamme@uantwerpen.be

Abstract

Mutations in *DAXX/ATRX*, *MEN1,* and genes involved in the phosphoinositide-3-kinase/Akt/mammalian target of rapamycin (PI3K/Akt/mTOR) pathway have been implicated in pancreatic neuroendocrine neoplasms (pNENs). However, mainly mutations present in the majority of tumor cells have been identified, while proliferation-driving mutations could be present only in small fractions of the tumor. This study aims to identify high- and low-abundance mutations in pNENs using ultra-deep targeted resequencing. Formalin-fixed paraffin-embedded matched tumor-normal tissue of 38 well-differentiated pNENs was sequenced using a HaloPlex targeted resequencing panel. Novel amplicon-based algorithms were used to identify both single nucleotide variants (SNVs) and insertion-deletions (indels) present in >10% of reads (high-abundance) and in <10% of reads (low-abundance). Found variants were validated by Sanger sequencing. Sequencing resulted in 416,711,794 reads with an average target base coverage of 2663±1476. Across all samples, 32 high-abundance somatic, 3 germline and 30 low-abundance mutations were withheld after filtering and validation. Overall, 92% of high-abundance and 84% of low-abundance mutations were predicted protein-damaging. Frequently mutated genes were *MEN1, DAXX*, *ATRX, TSC2,* PI3K/Akt/mTOR and MAPK-ERK pathway-related genes. Additionally, recurrent alterations on the same genomic position, so-called hotspot mutations, were found in *DAXX, PTCH2* and *CYFIP2*. This first ultra-deep sequencing study highlighted genetic intra-tumor heterogeneity in pNEN, by the presence of low-abundance mutations. The importance of the *ATRX/DAXX* pathway was confirmed by the first-ever pNEN-specific protein-damaging hotspot mutation in *DAXX.* In this study, both novel genes, including the pro-apoptotic *CYFIP2* gene and hedgehog-signaling *PTCH2*, and novel pathways, such as the MAPK-ERK pathway, were implicated in pNEN.

Introduction

Neuroendocrine neoplasms of the pancreas (pNENs), originating from the islet cells, are considered rare, although incidence is increasing (Dasari, et al. 2017). pNENs can occur as part of genetic syndromes, such as multiple neuroendocrine neoplasia 1 (MEN1), Von-Hippel Lindau (VHL) and tuberous sclerosis complex (TSC). However, most pNENs are sporadic tumors without familial history of NENs (Crona and Skogseid 2016). Recently, non-familial pNENs haven been genetically characterized using whole-exome and whole-genome sequencing in large cohorts of 40 to 102 patients (Jiao, et al. 2011; Sadanandam, et al. 2015; Scarpa, et al. 2017). These studies identified *MEN1* as most frequently mutated gene, in frequencies ranging from 37% to 44% of all sequenced tumors. Additionally, *DAXX* was found to be mutated in 22% to 25% of all tumor samples, while *ATRX* was mutated in 10% to 17% of all tumors. Menin (the *MEN1* protein), DAXX, and ATRX are epigenetic regulators. Menin is involved in histone modification, while ATRX and DAXX play a role in alternative telomere lengthening and chromatin remodeling (Elsasser, et al. 2011; Heaphy, et al. 2011). Additionally, mutations in genes involved in the phosphoinositide-3-kinase/Akt/mammalian target of rapamycin (PI3K/Akt/mTOR) pathway were found in 12% to 14% of tumors (Jiao et al. 2011; Scarpa et al. 2017). In the pivotal Radiant-3 trial, treatment with everolimus, an mTOR inhibitor, has demonstrated an improved progression-free survival in advanced pNENs (Yao, et al. 2011). Hence, alterations in the PI3K/Akt/mTOR pathway, such as mutations in *PTEN,* could have clinical implications. However, no molecular predictive biomarker for everolimus treatment has yet been identified. Frequent tumor-specific copy number alterations in *MEN1*, *ATRX*, *DAXX* an PI3K/Akt/mTOR genes implicate these core pathways further (Scarpa et al. 2017). Recent efforts to describe molecular subtypes, have led to the identification of five mutational signatures in pNEN, including the novel *MUTYH* signature

(Scarpa et al. 2017). However, in more than 50% of all tumors no dominant mutational signature could be identified (Scarpa et al. 2017). RNA expression analysis revealed three expression subtypes, respectively the insulinoma, MEN-1-like/intermediate and metastasis-like (MLP) subtype (Sadanandam et al. 2015; Scarpa et al. 2017). Clinical utility of these expression subtypes is subject of further study, as expression subtypes show a variable association with tumor grade, mainly in WHO 2010 grade 1 and 2 tumors (Sadanandam et al. 2015). Moreover, within-patient and within-tumor heterogeneity in proliferation has been demonstrated in neuroendocrine neoplasm models and patients (Shi, et al. 2015; Vandamme, et al. 2016; Vandamme, et al. 2015a). In recent pNEN sequencing studies, average sequencing depth was 61 to 102-fold (Sadanandam et al. 2015; Scarpa et al. 2017). Although covering all of the genome, these studies might lack sequencing power to reliably detect mutations present in a fraction of the cells, as these rare alleles might be present in less than 1 in 100 sequencing reads on a given genomic position (Gerstung, et al. 2012). Therefore, current studies lack information on mutational heterogeneity. By increasing sequencing depth, mutations, present in a fraction of cells, can be reliably identified (Gerstung et al. 2012). This study is the first to use an ultra-deep targeted resequencing approach in pNENs to elucidate mutations, present in less than 10% of sequencing reads.

Methods

Sample collection and clinical data

Patients, diagnosed between 1997 and 2013 with a reported WHO 2010 grade 1 or 2 pancreatic neuroendocrine neoplasm were retrospectively included in this study (Bosman, et al. 2010). Patients with a familial syndrome were excluded. Formalin-fixed paraffin-embedded (FFPE) samples of tumor and matched distant normal tissue, if available, of all

patients was collected at the Erasmus Medical Center (Rotterdam, the Netherlands) and the Antwerp University Hospital (Antwerp, Belgium). All samples were reviewed by a dedicated pathologist for histology, Ki67 index, mitoses per high power field and tumor purity. Only samples with estimated tumor purity >60% on hematoxylin and eosin (H&E) stained histological slide, after macrodissection, were included. Data on age, sex, TNM stage, age at diagnosis, secretion status, received treatments, disease-free survival and overall survival was collected. The study was approved by the institutional human ethics review board of the Antwerp University Hospital. Informed consent was obtained from all patients for the use of excess tissue material for scientific research, based on the opt-out registry to document the objection of patients (as specified in Belgian and Dutch law).

Targeted gene panel development

A custom HaloPlex enrichment panel (Agilent Technologies, Santa Clara, CA, VS) was developed to sequence all exons of 20 genes (**table 1)**. Genes were selected based upon patient and cell line sequencing results (Jiao et al. 2011; Vandamme, et al. 2015b). PI3K/Akt/mTOR pathway-related genes *MTOR, PTEN, PIK3CA* and *TSC2* mutations have been found in pNEN patients and could have therapeutic implications (Grabiner, et al. 2014; Jiao et al. 2011; Scarpa et al. 2017). The gene panel was extended with the PI3K-related *PIK3C2A* gene, as it was found mutated in pNEN cell line data (Vandamme et al. 2015b). Epigenetic modifiers could play a role in pNEN, as demonstrated by *MEN1, ATRX* and *DAXX* mutations identified previously in pNEN (Jiao et al. 2011; Scarpa et al. 2017). Next to these genes, *KANSL1* and *PIF1*, two epigenetic modifiers found in pNEN cell line data, were included in the panel (Vandamme et al. 2015b). As preclinical data suggests a role for the MAPK/ERK pathway in pNEN, *KRAS, MAP4K2, MAPK9* and *MAPKBP1* were added to the panel

(Valentino, et al. 2014; Vandamme et al. 2016). The *SMAD4* gene has been found mutated in neuroendocrine neoplasms, both in patient material and in cell lines (Bartsch, et al. 1999; Vandamme et al. 2015b). *TP53* and *CYFIP2* are two genes involved in apoptosis that are frequently implicated in oncogenesis. Both genes were found mutated in pNEN cell line data and were hence added to the panel (Vandamme et al. 2015b). Finally, the panel was extended with three genes (*KISS1, PTCH2, WNT1)* in known cancer-related pathways. All genes contained mutations in pNEN cell line data (Vandamme et al. 2015b). In our custom HaloPlex primer design, 99.59% of the 70,715 target kilobases of selected genes were covered by developed primers. The primer design was optimized for use with FFPE material and for sequencing on Illumina technology with a read length of 150 base pairs by increasing the number of amplicons to 19,838.

DNA isolation, HaloPlex enrichment and sequencing

After macrodissection, 10 slides of 5 µm of both tumor and normal tissue were used as input for DNA isolation using the QIAamp DNA FFPE Tissue Kit (Qiagen, Hilden, Germany), following manufacturer's instructions. The concentration of the isolated DNA was quantified using the Qubit 2.0 fluorometer with the dsDNA Broad Range Assay (Thermo Scientific, Wilmington, USA). To determine the amount of input DNA for HaloPlex enrichment, quality and degradation of the DNA were checked following the FFPE-Derived DNA Quality Assessment-protocol (Agilent Technologies, Santa Clara, CA, VS) using the LabChip GX (PerkinElmer, Waltham, MA, VS) with a High Sensitivity DNA kit (PerkinElmer, Waltham, MA, VS). Next, all tumor samples and three representative normal samples were prepared for targeted resequencing using a custom HaloPlex Design enrichment, optimized for FFPE sample enrichment, following the FFPE-optimized protocol according to manufacturer's

instructions. The enriched samples were hybridized, amplified and sequenced on two lanes of a paired-end flow cell using HiSeq 1500 (Illumina, San Diego, USA) platform in rapid run mode.

Read alignment, variant calling and filtering

Raw sequencing reads were analyzed using an in-house developed Perl-based workflow. First, FastQC software (version 1.0) was used to assess quality of the raw data (Andrews 2010). Adapters and low-quality bases were trimmed using Cutadapt (version 1.2.1) and an in-house developed paired-end read quality trimmer (Vandeweyer, et al. 2014), respectively. Paired-end reads were then aligned to the human reference genome (hg19, NCBI Build 37) using Burrows-Wheeler Aligner (BWA mem, version 0.7.3a) (Li and Durbin 2009). Picard (version 1.88) was used to mark and remove duplicates. Afterwards, the three aligned normals were merged using Samtools (version 0.1.18)(Li, et al. 2009). After merging, somatic variant calling was performed on the tumor aligned data with VarScan2 (version 2.3.9) using the three merged normals as one merged normal (Koboldt, et al. 2012). Alignments with mapping quality lower than 17 or nucleotides with base quality lower than 17 were ignored. The max per-BAM depth was set on 30,000 avoiding excessive memory usage. No correction for tumor purity was set during the somatic calling, purities were kept on default (100%). The variant calling files were first filtered using pyAmpli to eliminate false positive variants introduced by amplicon-based enrichment (Beyens, et al. 2017). All variants were annotated with ANNOVAR (Wang, et al. 2010), and filtered using VariantDB (Vandeweyer et al. 2014) according to different criteria (Results section). Identified variants were validated in tumor and its matching normal tissue, if available, with Sanger sequencing on the 3130xl Genetic Analyser (Applied Biosystems Inc., Foster City, VS) platform and analyzed using CLC DNA

Workbench v5 software (CLC Bio, Aarhus, Denmark). Data were visualized using the Maftools package (Mayakonda and Koeffler 2016) in R (version 3.3.3). Survival statistics were generated using the survival and survminer package for R (version 3.3.3).

Results

Patient characteristics

38 pNEN patients were included, of which 51% were male. Of the 38 included patients, 13 patients had a functional tumor (11 insulinomas, one gastrinoma and one glucagonoma). Mean age at diagnosis was 53 ± 14 years. Of all patients, 9 (16%) had metastatic disease at diagnosis (**suppl. table S1**). Tumor tissue was available for all included patients, while matched normal tissue was collected in 27 patients (71%). 24 patients were diagnosed with WHO grade 1 disease, while 13 patients had a WHO grade 2 tumor. Upon central pathology review, one patient was reclassified as a WHO 2010 grade 3 tumor, given the Ki67 index of 30%. Median follow-up time was 6.3 years (range: 1.9-19.2 years). Median overall survival was 13 years [95% confidence interval 11 years – not reached].

Genetic alterations in pancreatic neuroendocrine neoplasms

Targeted resequencing of the selected HaloPlex enrichment 20-gene panel (see materials and methods) resulted in a total of 416,711,794 reads, passing quality filtering, across 38 tumor samples and three normal samples. Of all reads, an average 80.4 ± 5.0% mapped on target regions. Average target base coverage was 2663 ± 1476 and 94.7 ± 1.9% of all target bases was covered at least 30 times. Using VarScan2, variants in the tumor were called

against three merged normal samples. Afterwards, the amplicon-based filtering method pyAmpli was deployed to withhold only alterations present in more than one amplicon (if more than one amplicon was in the enrichment design) (Beyens et al. 2017). Additionally, all variants that were marked as “somatic” by VarScan2 were withheld. By this combined elimination, genetic alterations that are inherent to the enrichment with the HaloPlex panel and, hence, appear in all amplicons across all samples, are removed as false positive. Additionally, genetic alterations that are present in all three sequenced normal samples will most likely not be oncogenic driver mutations. Hence, these mutations can be discarded as common polymorphisms or artefacts when they are seen in the tumor samples. After this combined filtering, 17 indels and 2270 single nucleotide variations (SNVs) were withheld in the 38 tumors. The resulting median mutation burden of 0.80 per Megabase (Mb, range 0.51-1.54) within the 20 selected genes, with a genomic length of 70.71 Mb, is in line with the previously reported genome-wide mutation burden of 0.82 per Mb in pNEN and is low in comparison to other tumor types (Scarpa et al. 2017). Although caution is needed when comparing mutation burden between the targeted sequencing panel and the previously reported whole-genome data, it seems that the 20 selected genes in the targeted panel show no enrichment for mutations in comparison to other genomic regions. Before further filtering, the median number of genetic alterations per tumor was 56 with the *MTOR* gene containing the most alterations (**figure 1**). The most frequent nucleotide substitutions were C <-> T transitions (**figure 1**). Across all samples, transitions made up 63.4% ± 2.3% of the filtered SNVs, resulting in a ratio of transitions to transversions of 1.74 ± 0.18 in the presented gene panel. In human germline samples, an average transitions to transversion rate of 1.7 is usually seen genome-wide (Lynch 2010). A genome-wide mutation spectrum with a predominant C to T/G to A transition pattern is seen in many adult cancers, including

melanoma, breast, lung, colorectal, ovarian and pancreas adenocarcinoma (Greenman, et al. 2007; Jones, et al. 2008). However, in pNENs a more even distribution of transversions and transitions has been reported previously, in line with the data in this study (Jiao et al. 2011).

Identification and validation of somatic and germline mutations

To identify mutations with possible functional impact, RefSeq synonymous as well as intronic SNVs and intronic indels were first removed from further analysis (Pruitt, et al. 2014). To eliminate common single nucleotide polymorphisms (SNPs), only variants with a minor allele frequency (MAF) smaller than 0.05 in the dbSNP v142, ESP65000 and 1000 Genomes databases were withheld (Genomes Project, et al. 2010; Sherry, et al. 2001). Final visual inspection of all remaining variants in Integrative Genomics Viewer (IGV version 2.2.5), led to the identification of 72 mutations with possible functional impact (**figure 2**) (Thorvaldsdottir, et al. 2012). Of these 72 mutations, 42 alterations were identified in more than 10% of sequencing reads at that genomic position and were considered high-abundance alterations. These 42 alterations were Sanger sequenced in tumor tissue. Additionally, of 27 patients (71%) corresponding normal tissue was available, allowing Sanger sequencing of normal tissue for 22 mutations. Out of the 42 high-abundant variants, 35 were validated through Sanger sequencing, while 6 variants could not be detected in the Sanger electropherogram traces. For one variant, PCR amplification of the tumor DNA region containing the variant was unsuccessful, despite successful amplification in control DNA and use of different primers. Overall, 83.3% of all high-abundant variants could be validated (**suppl. table S2**). The 35 validated mutations contained three germline RefSeq non-synonymous variants, one in *MAPKBP1* and two in *PIF1* respectively, all unique in three different tumors. None of the mutations were present in the cancer somatic mutation COSMIC v70 database (accession

235 date: 12th April 2017), while two SNVs were reported in the dbSNP142 database with
236 unknown clinical significance, respectively dbSNP142 rs139868280 (*PIF1*) and rs201725344
237 (*MAPKBP1*) (Forbes, et al. 2017; Sherry et al. 2001). The other *PIF1* chr15:g.65108822C>T
238 mutation was not found in any of the queried databases, including ExAc (version 03), 1000
239 Genomes Project (October 2014), dbSNP142 and COSMIC v70 (Forbes et al. 2017; Genomes
240 Project et al. 2010; Lek, et al. 2016; Sherry et al. 2001).
241

242 ## Abundant mutations include a *DAXX* and *CYFIP2* hotspot mutation

243 Of the 32 validated high-abundant somatic mutations, 21 SNVs were annotated as non-
244 synonymous by RefSeq, 6 as frameshift indels, 3 as stopgain SNVs, 1 as SNV in the 3'-UTR
245 and 1 as nonframeshift indel. The most commonly mutated gene was *DAXX* with five high-
246 abundance mutations, while four high-abundance mutations were found *MEN1, MAP4K2*
247 and *PTCH2*. *ATRX, KANSL1, TSC2* and *MAPKB1* each contained three high-abundance
248 mutations. These 8 genes accounted for 80% of all validated high-abundance mutations. No
249 high-abundance mutations were found in *PIF1, PIK3CA, PTEN, MAPK9, KRAS* and *TP53.* Using
250 variantDB, all variants were annotated for functional impact prediction using the
251 MutationAssesor, MutationTaster, Provean and PolyPhen algorithms (Vandeweyer et al.
252 2014). Of all variants, 92.0% was predicted damaging by at least one algorithm, while 36.0%
253 was predicted damaging by at least 3 algorithms. Three mutations were also seen in other
254 tumor types, according the COSMIC database (Forbes et al. 2017). Two recurrent, so-called
255 hotspot, mutations were found, one in *CYFIP2* and one in *DAXX.* The *CYFIP2* non-
256 synonymous variant g.156766140G>A (NM_001037333, p.D820N) was found in two pNEN
257 tumors. This variant had previously been identified in skin squamous cell carcinoma,
258 according to COSMIC, and was predicted to be damaging by MutationTaster and PROVEAN

(Choi, et al. 2012; Schwarz, et al. 2014). Within the *DAXX* gene, one genomic position was altered differently in two tumors, yielding the non-synonymous g.33289247G>A (NM_001141970.1, p.S102L) and the stopgain g.33289247G>T (NM_001141970.1, p.S102X) mutations. Both mutations were predicted damaging by all used prediction algorithms, pointing towards a very likely *DAXX* loss-of-function in these tumors. The non-synonymous g.33289247G>A *DAXX* mutations has previously been found as a somatic mutation in one lung squamous cell carcinoma, according to COSMIC.

Low-abundance mutations contain a hotspot mutation in *PTCH2*

Next to high-abundance mutations, 30 mutations were found in less than 10% of targeted resequencing reads in tumor tissue. These mutations are considered low-abundance mutations. As the detection limit of Sanger sequencing is around 10%, these low-abundant alterations could not be Sanger sequenced (Tsiatis, et al. 2010). However, the Sanger sequencing validation rate of 83% in the high-abundant mutations demonstrates that the used combined filtering strategy (see above) yields mainly true positives. Additionally, only 9% of validated mutations was present in corresponding normal samples, illustrating that the employed filtering strategy selects for somatic variants. Hence, we assume that most of the low-abundance mutations are also both valid and somatic. RefSeq annotated 21 of these 30 low-abundance mutations as non-synonymous SNVs, four as frameshift indels, three as stopgain SNVs , one as splicing SNV and one as SNV in the 3'-UTR. The 3'-UTR *PIK3C2A* g.17111197_17111198del was found in 3 tumors. In addition, 2 intronic variants were found, the *DAXX* g.33286734A>C which was seen in 8 pNENs, and the TSC2 g.2124481_2124482insG, identified in 5 tumors. However, functional impact of these intronic mutations remains unclear. When predicting protein impact on the 26 exonic SNVs

with the MutationAssesor, MutationTaster, Provean and PolyPhen algorithms using variantDB, 84.0% of all SNVs was predicted damaging by at least one algorithm, while 52.0% was predicted damaging by three or more prediction algorithms (Vandeweyer et al. 2014). After inclusion of the four frameshift indels, which can be considered to have a deleterious impact on protein function, 86.6% of all mutations have a likely protein impact. Three mutations were previously found in cancer samples, according to the COSMIC database, including the non-synonymous *TP53* g.7578457C>T mutation (NM_001276695.1, p.R158H) which was identified in 36 tumors of various origin (Forbes et al. 2017). Two tumors contained the same stopgain g.45292871C>A mutation (NM_001166292, p.G828X) in *PTCH2*, predicted to be damaging by MutationTaster, PROVEAN and SIFT. This protein-damaging *PTCH2* mutation is hence a novel low-abundance hotspot mutation within pNEN.

Mutational signatures in pNEN

In total, 32 tumors contained mutations while 6 tumors had no mutations that survived filtering (**figure 3**). Both low-abundance and high-abundance mutations were seen in 11 tumors (29%). High-abundance mutations were seen exclusively in 14 tumors (37%), while 7 tumors (18%) only contained low-abundance mutations (**figure 2**). *MEN1* was mutated most frequently in 8 out of 38 tumors (21%). *DAXX* and *ATRX* were both mutated in 5 out of 38 tumors (13%). The PI3K/Akt/mTOR-related gene *TSC2* was mutated in 7 out of 38 tumors (18%). Overall, mutations in PI3K/Akt/mTOR-related genes were seen in 29% of the tumors, including a validated non-synonymous g.1308007C>T mutation in *MTOR* (NM_004958, p.A329T, rs35903812) not previously reported in pNEN. The mitogen-activated kinase and

extracellular signal-regulated kinase (MAPK-ERK pathway) genes *MAP4K2* and *MAPKBP1* were each mutated in three tumors.

Discussion

This study presents the first ultra-deep targeted resequencing of pNENs in archival tissue. The relative rarity of pNENs has led to only a limited number of large-scale studies on the genetic constitution of pNENs (Jiao et al. 2011; Sadanandam et al. 2015; Scarpa et al. 2017). Additionally, these studies focus on a broad overview of frequent genetic alterations in pNEN and report high-abundance mutations. These high-abundance mutations are present in the majority of tumors cells. However, various studies have demonstrated that the genetic make-up of primary tumors evolves dynamically in time (Burrell, et al. 2013; Stratton, et al. 2009). This time-dependent change of the genetic alterations present in a tumor reflects the appearance and disappearance of subsets of tumor cells, so-called subclones, within one tumor (Burrell et al. 2013; Stratton et al. 2009). In our study, the use of ultra-deep sequencing allowed for the identification of genetic alterations that are present in a low fraction of the tumoral tissue, so-called low-abundance mutations. These low-abundance mutations are indicative for the genetic heterogeneity within a single tumor. Recent genetic studies have identified the insulinoma, MEN-1-like/intermediate and metastasis-like (MLP) RNA expression subtype in pNENs (Sadanandam et al. 2015). Although the MEN-1-like tumors frequently contains *MEN1* mutations, the mutational burden of high-abundance mutations in other core pathways seems to be more variable across subtypes (Sadanandam et al. 2015). Additionally, DNA damage repair, chromatin modification, alternated telomere length and the PI3K/Akt/mTOR pathways have been highlighted as core altered pathways in pNEN (Jiao et al. 2011; Scarpa et al. 2017). In this study, we demonstrate that low-

328 abundance mutations are found in these pathways. Hence, low-abundance mutations might
329 help to better classify tumors. However, validation of these low-abundance mutations
330 remains complex and its lack forms a limitation of our study. The gene with the most high-
331 abundance mutations within our study was the tumor suppressor gene *DAXX*. ATRX and
332 DAXX form a complex facilitating the incorporation of histone variant H3.3 at the telomeres
333 and, consequently, play a role in alternative lengthening of telomeres (Heaphy et al. 2011;
334 Lewis, et al. 2010). In many cancer types, it has been demonstrated that alternative
335 telomere lengthening (ATL) leads to a prolonged cell survival, which is a hallmark of cancer
336 (Cesare and Reddel 2010). In pNEN, ATL has been associated with a reduced disease-free
337 survival (Singhi, et al. 2017). Additionally, loss of ATRX and DAXX on immunohistochemistry
338 (IHC) staining, caused by inactivating mutations or copy number loss, is associated with
339 increased occurrence of metastasis and reduced disease-free survival (Scarpa et al. 2017;
340 Singhi et al. 2017). Both high- and low-abundance mutations in *DAXX* and *ATRX* were
341 identified in this study, including the first-ever validated recurrent, hotspot, mutation in
342 *DAXX*, with likely loss-of-function on protein level. In line with other studies, exonic
343 (transcript coding or protein encoding) mutations in *DAXX* and *ATRX* were mutually exclusive
344 (Jiao et al. 2011; Scarpa et al. 2017). As this is the first study to demonstrate the existence of
345 low-abundance mutations in *ATRX* and *DAXX*, conclusions on clinical impact are limited.
346 Nonetheless, detection of low-abundance mutations might lead to the identification of DAXX
347 and ATRX loss before this is apparent on IHC and, thus, an earlier identification of high-risk
348 patients. Given the low number of events in the studied population (both in disease-
349 recurrence and in mortality), this study is not adequately powered to evaluate prognostic
350 relevance of these low-abundance mutations. Hence, further studies are needed. Menin, the
351 nuclear protein encoded by *MEN1,* impacts ATL by negatively regulating hTERT (Lin and

Elledge 2003). Additionally, it plays a key role in chromatin remodeling and gene expression through histone acetylation and deacetylation (Kim, et al. 2003). *MEN1* mutations have been implicated in pNEN oncogenesis, both as part of the familial MEN1 syndrome, and in sporadic tumors (Corbo, et al. 2010; Crona and Skogseid 2016; Jiao et al. 2011; Scarpa et al. 2017). In 12-14% of all pNEN patients, a mutation in PI3K/Akt/mTOR-related genes is reported, including mutations in *PTEN, MTOR, DEPDC5, TSC1, TSC2* and *PIK3CA* (Chou, et al. 2016; Jiao et al. 2011; Scarpa et al. 2017). In this study, PI3K/Akt/mTOR-related mutations could be identified in 29% of all tumors, including a novel p.A329T mutation in *MTOR* in pNEN. This increased frequency of mutations in the PI3K/Akt/mTOR-related genes is due to the detection of low-abundance mutations in these tumor samples. The relation of everolimus efficacy and PI3K/Akt/mTOR pathway-related mutations remains the subject of study in pNEN. However, in other cancer types, mutations of the PI3K/Akt/mTOR pathways seems to confer everolimus sensitivity (Grabiner et al. 2014; Wagle, et al. 2014). In neuroendocrine neoplasms and other cancer types, cross-talk activation between the PI3K/Akt/mTOR pathway and the mitogen-activated kinase and extracellular signal-regulated kinase (MAPK-ERK pathway) through PI3K has been described (Carracedo, et al. 2008; Valentino et al. 2014; Zitzmann, et al. 2010). Until now, no mutations in MAPK-ERK pathway-related genes have been reported in pNEN. In this study, mutations in *MAP4K2* and *MAPKBP1* were identified, further implicating this pathway in pNEN and providing additional rationale for the use of MEK-inhibitors in pNEN, either in combination with mTOR inhibitors or alone. Although *TP53* is frequently mutated in other cancers, *TP53* mutation frequency is low in pNEN, as demonstrated by only two low-abundance *TP53* mutations being present in our cohort (Jiao et al. 2011; Scarpa et al. 2017). Additionally, the pro-apoptotic gene *CYFIP2* was mutated in four tumors. In two tumors, the exact same mutation was present, a so-

called hotspot mutation. This validated mutation has never been reported before in pNEN and is predicted to be protein-damaging, warranting further studies into the role of *CYFIP2* in pNEN. Three mutations (one high-abundance and two low-abundance) were found in *SMAD4*. Unlike in small intestinal neuroendocrine neoplasms, where *SMAD4* loss is relatively common, the frequency of *SMAD4* mutations in pNEN has been the matter of debate (Banck, et al. 2013; Bartsch et al. 1999; Perren, et al. 2003). Multiple low-abundance recurrent mutations were identified, including a hotspot mutation in *PTCH2. PTCH2* encodes the Patched 2 protein, which is involved in hedgehog signaling (Rahnama, et al. 2004; Smyth, et al. 1999). *PTCH2* mutations haven been found in basal cell carcinoma, medulloblastoma and rhabdomyosarcoma and myeloproliferative neoplasms (Klein, et al. 2016; Smyth et al. 1999; Taeubner, et al. 2018). However, this is the first time that hedgehog signaling has been implicated in pNENs. As the technical limitations of Sanger sequencing didn't allow validation of this low-abundance mutation, further studies in replication cohorts are needed to confirm hedgehog signaling as a novel pathway in pNENs. Given that various hedgehog signaling inhibitors have been approved for use in basal cell carcinoma, confirmatory studies on the role of hedgehog signaling could open new therapeutic options for pNENs, harboring *PTCH2* mutations (Lacouture, et al. 2016). Finally, the limited availability of fresh-frozen tissue in pNEN could hinder the implementation of next-generation sequencing technology in pNEN diagnostics. In contrast, archival tissue, necessary for histological diagnosis of pNEN, is frequently available and can be easily manipulated and stored in a cost-effective manner. A possible limitation of the use of FFPE, is the induction of false-positive mutations by formalin fixation (Williams, et al. 1999). These mutations often follow a deamination pattern, resulting in transitions (C>T or G>A). Hence, when formalin fixation would result in a considerable number of additional induced mutations, there would be an increase in the

number of transitions (C>T or G>A) in comparison to transversions (A>C or G>T). However, the ratio of transitions to transversion in this study is similar to transition-transversion ratios seen in normal human (germline) samples and in pancreatic neuroendocrine neoplasm samples from fresh-frozen tissue (Jiao et al. 2011). Therefore, the impact of formalin-fixation can be considered to be relatively limited. To further reduce any potential impact, the in-house developed pyAmpli tool filters specifically for mutations present in more than one amplicon and, thus, amplified DNA fragment (Beyens et al. 2017). As fixation-induced "deamination" is stochastic and happens randomly in all DNA strands, the chance that two different DNA molecules have exactly the same formalin fixation-induced is very limited. Hence, our study demonstrates that by using this approach archival FFPE tissue can be used reliably in genetic analysis of pNENs.

In conclusion, this study adds to the growing body of evidence on the broad genetic constitution of pNENs by demonstrating the presence of low-abundance mutations and genetic heterogeneity in pNENs. We highlight the importance of the *ATRX/DAXX* pathway by reporting the first-ever pNEN-specific protein-damaging hotspot mutation in *DAXX*, and uncover novel genes and pathways involved in pNENs, including pro-apoptotic *CYFIP2,* hedgehog signaling and the MAPK-ERK pathway.

Declaration of interest

Timon Vandamme: advisory role and speakers' fees for Ipsen and Novartis.

Wouter de Herder: advisory role and speakers' fees for Ipsen and Novartis.

Marc Peeters: advisory role and speakers' fees for Ipsen and Novartis.

Matthias Beyens, Ken Op de Beeck, Fadime Dogan, Peter M. van Koetsveld, Patrick Pauwels, Guy Van Camp, Leo J. Hofland, Gitta Boons, Anne Schepers, Kimberley Kamp, Katharina Biermann: No conflicts of interest to declare

Funding

This work was supported by the Flemish Agency of Scientifc Research (FWO grant G.0327.13N) and the ENETS-Ipsen 2013 Translational Research Fellowship.

Author contributions

TV, MB, GB, AS performed the sequencing experiments. TV, MB, KOdB processed the experimental data, performed the analysis, drafted the manuscript and designed the figures. PP, KB and LH performed pathological review of all tumor and normal samples and aided in patient selection. KK and WW aided in patient selection and collected clinicopathogical data. LH, WW, MP and GVC were involved in planning and supervised the work. All authors discussed the results and commented on the manuscript.

Acknowledgements

We would like to thank Lesley De Backer from the Multidisciplinair Oncologisch Centrum Antwerpen (MOCA) and NETwerk for her support in collecting clinicopathological data of all patients included at the University Hospital Antwerp.

References

Andrews S 2010 FastQC: a quality control tool for high throughput sequence data.

Banck MS, Kanwar R, Kulkarni AA, Boora GK, Metge F, Kipp BR, Zhang L, Thorland EC, Minn KT, Tentu R, et al. 2013 The genomic landscape of small intestine neuroendocrine tumors. *J Clin Invest* **123** 2502-2508.

Bartsch D, Hahn SA, Danichevski KD, Ramaswamy A, Bastian D, Galehdari H, Barth P, Schmiegel W, Simon B & Rothmund M 1999 Mutations of the DPC4/Smad4 gene in neuroendocrine pancreatic tumors. *Oncogene* **18** 2367-2371.

Beyens M, Boeckx N, Van Camp G, Op de Beeck K & Vandeweyer G 2017 pyAmpli: an amplicon-based variant filter pipeline for targeted resequencing data. *BMC Bioinformatics* **18** 554.

Bosman FT, Carneiro F, Hruban RH & Theise ND 2010 *WHO classification of tumours of the digestive system.* Lyon: IARC Press.

Burrell RA, McGranahan N, Bartek J & Swanton C 2013 The causes and consequences of genetic heterogeneity in cancer evolution. *Nature* **501** 338-345.

Carracedo A, Ma L, Teruya-Feldstein J, Rojo F, Salmena L, Alimonti A, Egia A, Sasaki AT, Thomas G, Kozma SC, et al. 2008 Inhibition of mTORC1 leads to MAPK pathway activation through a PI3K-dependent feedback loop in human cancer. *J Clin Invest* **118** 3065-3074.

Cesare AJ & Reddel RR 2010 Alternative lengthening of telomeres: models, mechanisms and implications. *Nat Rev Genet* **11** 319-330.

Choi Y, Sims GE, Murphy S, Miller JR & Chan AP 2012 Predicting the functional effect of amino acid substitutions and indels. *PLoS One* **7** e46688.

Chou WC, Lin PH, Yeh YC, Shyr YM, Fang WL, Wang SE, Liu CY, Chang PM, Chen MH, Hung YP, et al. 2016 Genes involved in angiogenesis and mTOR pathways are frequently mutated in Asian patients with pancreatic neuroendocrine tumors. *Int J Biol Sci* **12** 1523-1532.

Corbo V, Dalai I, Scardoni M, Barbi S, Beghelli S, Bersani S, Albarello L, Doglioni C, Schott C, Capelli P, et al. 2010 MEN1 in pancreatic endocrine tumors: analysis of gene and protein status in 169 sporadic neoplasms reveals alterations in the vast majority of cases. *Endocr Relat Cancer* **17** 771-783.

Crona J & Skogseid B 2016 GEP- NETS UPDATE: Genetics of neuroendocrine tumors. *Eur J Endocrinol* **174** R275-290.

Dasari A, Shen C, Halperin D, Zhao B, Zhou S, Xu Y, Shih T & Yao JC 2017 Trends in the Incidence, Prevalence, and Survival Outcomes in Patients With Neuroendocrine Tumors in the United States. *JAMA Oncol* **3** 1335-1342.

Elsasser SJ, Allis CD & Lewis PW 2011 Cancer. New epigenetic drivers of cancers. *Science* **331** 1145-1146.

Forbes SA, Beare D, Boutselakis H, Bamford S, Bindal N, Tate J, Cole CG, Ward S, Dawson E, Ponting L, et al. 2017 COSMIC: somatic cancer genetics at high-resolution. *Nucleic Acids Res* **45** D777-D783.

Genomes Project C, Abecasis GR, Altshuler D, Auton A, Brooks LD, Durbin RM, Gibbs RA, Hurles ME & McVean GA 2010 A map of human genome variation from population-scale sequencing. *Nature* **467** 1061-1073.

Gerstung M, Beisel C, Rechsteiner M, Wild P, Schraml P, Moch H & Beerenwinkel N 2012 Reliable detection of subclonal single-nucleotide variants in tumour cell populations. *Nat Commun* **3** 811.

489 Grabiner BC, Nardi V, Birsoy K, Possemato R, Shen K, Sinha S, Jordan A, Beck AH & Sabatini
490 DM 2014 A diverse array of cancer-associated MTOR mutations are hyperactivating and can
491 predict rapamycin sensitivity. *Cancer Discov* **4** 554-563.
492 Greenman C, Stephens P, Smith R, Dalgliesh GL, Hunter C, Bignell G, Davies H, Teague J,
493 Butler A, Stevens C, et al. 2007 Patterns of somatic mutation in human cancer genomes.
494 *Nature* **446** 153-158.
495 Heaphy CM, de Wilde RF, Jiao Y, Klein AP, Edil BH, Shi C, Bettegowda C, Rodriguez FJ,
496 Eberhart CG, Hebbar S, et al. 2011 Altered telomeres in tumors with ATRX and DAXX
497 mutations. *Science* **333** 425.
498 Jiao Y, Shi C, Edil BH, de Wilde RF, Klimstra DS, Maitra A, Schulick RD, Tang LH, Wolfgang CL,
499 Choti MA, et al. 2011 DAXX/ATRX, MEN1, and mTOR pathway genes are frequently altered in
500 pancreatic neuroendocrine tumors. *Science* **331** 1199-1203.
501 Jones S, Zhang X, Parsons DW, Lin JC, Leary RJ, Angenendt P, Mankoo P, Carter H, Kamiyama
502 H, Jimeno A, et al. 2008 Core signaling pathways in human pancreatic cancers revealed by
503 global genomic analyses. *Science* **321** 1801-1806.
504 Kim H, Lee JE, Cho EJ, Liu JO & Youn HD 2003 Menin, a tumor suppressor, represses JunD-
505 mediated transcriptional activity by association with an mSin3A-histone deacetylase
506 complex. *Cancer Res* **63** 6135-6139.
507 Klein C, Zwick A, Kissel S, Forster CU, Pfeifer D, Follo M, Illert AL, Decker S, Benkler T, Pahl H,
508 et al. 2016 Ptch2 loss drives myeloproliferation and myeloproliferative neoplasm
509 progression. *J Exp Med* **213** 273-290.
510 Koboldt DC, Zhang Q, Larson DE, Shen D, McLellan MD, Lin L, Miller CA, Mardis ER, Ding L &
511 Wilson RK 2012 VarScan 2: somatic mutation and copy number alteration discovery in
512 cancer by exome sequencing. *Genome Res* **22** 568-576.

513 Lacouture ME, Dreno B, Ascierto PA, Dummer R, Basset-Seguin N, Fife K, Ernst S, Licitra L,
514 Neves RI, Peris K, et al. 2016 Characterization and Management of Hedgehog Pathway
515 Inhibitor-Related Adverse Events in Patients With Advanced Basal Cell Carcinoma. *Oncologist*
516 **21** 1218-1229.
517 Lek M, Karczewski KJ, Minikel EV, Samocha KE, Banks E, Fennell T, O'Donnell-Luria AH, Ware
518 JS, Hill AJ, Cummings BB, et al. 2016 Analysis of protein-coding genetic variation in 60,706
519 humans. *Nature* **536** 285-291.
520 Lewis PW, Elsaesser SJ, Noh KM, Stadler SC & Allis CD 2010 Daxx is an H3.3-specific histone
521 chaperone and cooperates with ATRX in replication-independent chromatin assembly at
522 telomeres. *Proc Natl Acad Sci U S A* **107** 14075-14080.
523 Li H & Durbin R 2009 Fast and accurate short read alignment with Burrows-Wheeler
524 transform. *Bioinformatics* **25** 1754-1760.
525 Li H, Handsaker B, Wysoker A, Fennell T, Ruan J, Homer N, Marth G, Abecasis G, Durbin R &
526 Genome Project Data Processing S 2009 The Sequence Alignment/Map format and
527 SAMtools. *Bioinformatics* **25** 2078-2079.
528 Lin SY & Elledge SJ 2003 Multiple tumor suppressor pathways negatively regulate
529 telomerase. *Cell* **113** 881-889.
530 Lynch M 2010 Rate, molecular spectrum, and consequences of human mutation. *Proc Natl*
531 *Acad Sci U S A* **107** 961-968.
532 Mayakonda A & Koeffler P 2016 Maftools: Efficient analysis, visualization and summarization
533 of MAF files from large-scale cohort based cancer studies. *BioRxiv*.
534 Perren A, Saremaslani P, Schmid S, Bonvin C, Locher T, Roth J, Heitz PU & Komminoth P 2003
535 DPC4/Smad4: no mutations, rare allelic imbalances, and retained protein expression in
536 pancreatic endocrine tumors. *Diagn Mol Pathol* **12** 181-186.

537 Pruitt KD, Brown GR, Hiatt SM, Thibaud-Nissen F, Astashyn A, Ermolaeva O, Farrell CM, Hart
538 J, Landrum MJ, McGarvey KM, et al. 2014 RefSeq: an update on mammalian reference
539 sequences. *Nucleic Acids Res* **42** D756-763.
540 Rahnama F, Toftgard R & Zaphiropoulos PG 2004 Distinct roles of PTCH2 splice variants in
541 Hedgehog signalling. *Biochem J* **378** 325-334.
542 Sadanandam A, Wullschleger S, Lyssiotis CA, Grotzinger C, Barbi S, Bersani S, Korner J, Wafy
543 I, Mafficini A, Lawlor RT, et al. 2015 A Cross-Species Analysis in Pancreatic Neuroendocrine
544 Tumors Reveals Molecular Subtypes with Distinctive Clinical, Metastatic, Developmental,
545 and Metabolic Characteristics. *Cancer Discov* **5** 1296-1313.
546 Scarpa A, Chang DK, Nones K, Corbo V, Patch AM, Bailey P, Lawlor RT, Johns AL, Miller DK,
547 Mafficini A, et al. 2017 Whole-genome landscape of pancreatic neuroendocrine tumours.
548 *Nature*.
549 Schwarz JM, Cooper DN, Schuelke M & Seelow D 2014 MutationTaster2: mutation prediction
550 for the deep-sequencing age. *Nat Methods* **11** 361-362.
551 Sherry ST, Ward MH, Kholodov M, Baker J, Phan L, Smigielski EM & Sirotkin K 2001 dbSNP:
552 the NCBI database of genetic variation. *Nucleic Acids Res* **29** 308-311.
553 Shi C, Gonzalez RS, Zhao Z, Koyama T, Cornish TC, Hande KR, Walker R, Sandler M, Berlin J &
554 Liu EH 2015 Liver metastases of small intestine neuroendocrine tumors: Ki-67 heterogeneity
555 and World Health Organization grade discordance with primary tumors. *Am J Clin Pathol* **143**
556 398-404.
557 Singhi AD, Liu TC, Roncaioli JL, Cao D, Zeh HJ, Zureikat AH, Tsung A, Marsh JW, Lee KK, Hogg
558 ME, et al. 2017 Alternative Lengthening of Telomeres and Loss of DAXX/ATRX Expression
559 Predicts Metastatic Disease and Poor Survival in Patients with Pancreatic Neuroendocrine
560 Tumors. *Clin Cancer Res* **23** 600-609.

561 Smyth I, Narang MA, Evans T, Heimann C, Nakamura Y, Chenevix-Trench G, Pietsch T,
562 Wicking C & Wainwright BJ 1999 Isolation and characterization of human patched 2 (PTCH2),
563 a putative tumour suppressor gene inbasal cell carcinoma and medulloblastoma on
564 chromosome 1p32. *Hum Mol Genet* **8** 291-297.
565 Stratton MR, Campbell PJ & Futreal PA 2009 The cancer genome. *Nature* **458** 719-724.
566 Taeubner J, Brozou T, Qin N, Bartl J, Ginzel S, Schaper J, Felsberg J, Fulda S, Vokuhl C,
567 Borkhardt A, et al. 2018 Congenital embryonal rhabdomyosarcoma caused by heterozygous
568 concomitant PTCH1 and PTCH2 germline mutations. *Eur J Hum Genet* **26** 137-142.
569 Thorvaldsdottir H, Robinson JT & Mesirov JP 2012 Integrative Genomics Viewer (IGV): high-
570 performance genomics data visualization and exploration. *Brief Bioinform*.
571 Tsiatis AC, Norris-Kirby A, Rich RG, Hafez MJ, Gocke CD, Eshleman JR & Murphy KM 2010
572 Comparison of Sanger sequencing, pyrosequencing, and melting curve analysis for the
573 detection of KRAS mutations: diagnostic and clinical implications. *J Mol Diagn* **12** 425-432.
574 Valentino JD, Li J, Zaytseva YY, Mustain WC, Elliott VA, Kim JT, Harris JW, Campbell K, Weiss
575 HL, Wang C, et al. 2014 Co-Targeting the PI3K and RAS Pathways for the Treatment of
576 Neuroendocrine Tumors. *Clin Cancer Res*.
577 Vandamme T, Beyens M, de Beeck KO, Dogan F, van Koetsveld PM, Pauwels P, Mortier G,
578 Vangestel C, de Herder W, Van Camp G, et al. 2016 Long-term acquired everolimus
579 resistance in pancreatic neuroendocrine tumours can be overcome with novel PI3K-AKT-
580 mTOR inhibitors. *British Journal of Cancer* **114** 650-658.
581 Vandamme T, Beyens M, Peeters M, Van Camp G & Op de Beeck K 2015a Next generation
582 exome sequencing of pancreatic neuroendocrine tumor cell lines BON-1 and QGP-1 reveals
583 different lineages. *Cancer Genetics* **208** 523-523.

584 Vandamme T, Peeters M, Dogan F, Pauwels P, Van Assche E, Beyens M, Mortier G,
585 Vandeweyer G, de Herder W, Van Camp G, et al. 2015b Whole-exome characterization of
586 pancreatic neuroendocrine tumor cell lines BON-1 and QGP-1. *J Mol Endocrinol* **54** 137-147.
587 Vandeweyer G, Van Laer L, Loeys B, Van den Bulcke T & Kooy RF 2014 VariantDB: a flexible
588 annotation and filtering portal for next generation sequencing data. *Genome Med* **6** 74.
589 Wagle N, Grabiner BC, Van Allen EM, Amin-Mansour A, Taylor-Weiner A, Rosenberg M, Gray
590 N, Barletta JA, Guo Y, Swanson SJ, et al. 2014 Response and acquired resistance to
591 everolimus in anaplastic thyroid cancer. *N Engl J Med* **371** 1426-1433.
592 Wang K, Li M & Hakonarson H 2010 ANNOVAR: functional annotation of genetic variants
593 from high-throughput sequencing data. *Nucleic Acids Res* **38** e164.
594 Williams C, Ponten F, Moberg C, Soderkvist P, Uhlen M, Ponten J, Sitbon G & Lundeberg J
595 1999 A high frequency of sequence alterations is due to formalin fixation of archival
596 specimens. *Am J Pathol* **155** 1467-1471.
597 Yao JC, Shah MH, Ito T, Bohas CL, Wolin EM, Van Cutsem E, Hobday TJ, Okusaka T, Capdevila
598 J, de Vries EG, et al. 2011 Everolimus for advanced pancreatic neuroendocrine tumors. *N*
599 *Engl J Med* **364** 514-523.
600 Zitzmann K, Ruden J, Brand S, Goke B, Lichtl J, Spottl G & Auernhammer CJ 2010
601 Compensatory activation of Akt in response to mTOR and Raf inhibitors - a rationale for dual-
602 targeted therapy approaches in neuroendocrine tumor disease. *Cancer Lett* **295** 100-109.
603
604

Table legends

Table 1. List of genes (including encoded protein, chromosomal positions and number of exons) and the calculated coverage of the custom HaloPlex enrichment panel. * Multifunctional protein also associated with FAS signaling pathway.

Figure legends

Figure 1. Summary plot of SNVs (*N*=2270), insertions (*N*=9) and deletions (*N*=8) of all 38 samples, after amplicon-based filtering.

Figure 2. Filter strategy and abundancy of mutations across tumors. Filtered variants are SNVs or indels that are not RefSeq synonymous or intronic and have a minor allele frequency (MAF) ≤ 0.05 in dbSNP v142, ESP65000 and 1000 Genomes. Abundance is considered low for alterations found in <10% of targeted resequencing reads in tumor tissue and high when an alteration is present in ≥10% of targeted resequencing reads. Mutation are validated somatic when mutation is present in Sanger sequencing of tumor but not in normal (if available). Germline mutations are present in Sanger sequencing traces of both tumor and normal tissue. Not validated SNVs are those SNVs with absent Sanger traces or inconclusive results. All low-abundance SNVs or indels are assumed to be somatic. Pie-chart shows the percentage of patients whose tumors contained only low-abundance mutations (grey), only high-abundance mutations (yellow), both (red) or no mutations (blue).

Figure 3. Mutation plot showing frequency, type of mutations, abundancy and mutational distribution of genetic alterations across 38 included tumors, after filtering and validation (if

executed), including both high-abundance (*N*=32) and low-abundance (*N*=30) mutations. Low-abundance mutations are marked with red, in addition to color-coded mutation type. When a tumor contains multiple mutations within one gene, this is annotated as multi-hit (dark green).

RefSeq gene id	Encoded protein	Chromosomal position	Exons	Size (bp)	Coverage (%)
PI3K/AKT/mTOR pathway					
MTOR	Mechanistic target of rapamycin	chr1:11166651-11319476	60	9217	99.75
PIK3C2A	Phosphatidylinositol-4-phosphate 3-kinase catalytic subunit type 2 alpha	chr11:17111274-17191298	32	5705	100
PIK3CA	Phosphatidylinositol-4,5-bisphosphate 3-kinase catalytic subunit alpha	chr3:178916603-178952162	20	3609	99.5
PTEN	Phosphatase and tensin homolog	chr10:89624216-89725239	9	1392	100
TSC2	Tuberous sclerosis 2	chr16:2098260-2138621	43	6592	98.07
Transcription/chromatin remodeling					
ATRX	ATRX, chromatin remodeler	chrX:76763818-77041497	37	8299	99.92
*DAXX**	Death domain associated protein	chr6:33286509-33290701	8	2436	100
KANSL1	KAT8 regulatory NSL complex subunit 1	chr17:44108831-44249519	14	3598	100
MEN1	Menin 1	chr11:64571795-64577591	9	2028	100
PIF1	PIF1 5'-to-3' DNA helicase	chr15:65107879-65116544	13	2444	100
MAPK/ERK pathway					
KRAS	KRAS proto-oncogene, GTPase	chr12:25362718-25398328	6	828	100
MAP4K2	Mitogen-activated protein kinase kinase kinase kinase 2	chr11:64556998-64570631	32	3103	100
MAPK9	Mitogen-activated protein kinase 9	chr5:179663373-179707571	14	1943	100
MAPKBP1	Mitogen-activated protein kinase binding protein 1	chr15:42067463-42117644	32	5461	100
p53 pathway					
CYFIP2	Cytoplasmic FMR1 Interacting Protein 2	chr5:156712361-156820018	34	4543	99.89
TP53	Tumor protein p53	chr17:7565246-7579922	14	1697	97.88
G protein–coupled receptor (GPCR) signaling pathway					
KISS1	KiSS-1 metastasis-suppressor	chr1:204159601-204162014	2	457	100
Hedgehog signaling pathway					
PTCH2	Patched 2	chr1:45286350-45308614	24	4171	100
TGF-β signaling pathway					
SMAD4	SMAD family member 4	chr18:48573406-48604847	13	1999	100
Wnt signaling pathway					
WNT1	Wnt family member 1	chr12:49372423-49375433	4	1193	100

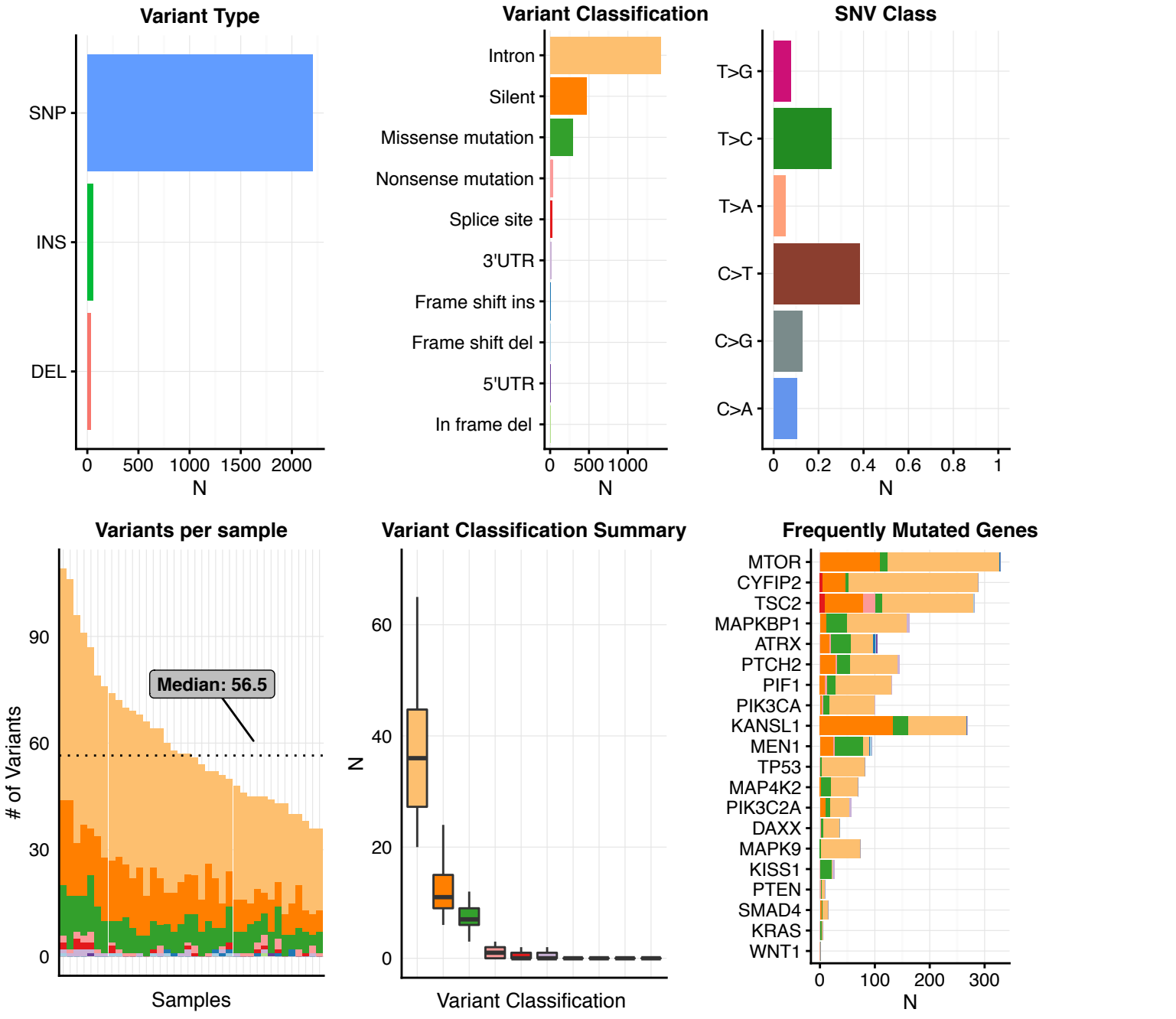
Variant Type
SNP
INS
DEL
0
500
1000
1500
2000
N
Variant Classification
Intron
Silent
Missense mutation
Nonsense mutation
Splice site
3'UTR
Frame shift ins
Frame shift del
5'UTR
In frame del
0
500
1000
N
SNV Class
T>G
T>C
T>A
C>T
C>G
C>A
0
0.2
0.4
0.6
0.8
1
N
Variants per sample
Median: 56.5
# of Variants
90
60
30
0
Samples
Variant Classification Summary
N
60
40
20
0
Variant Classification
Frequently Mutated Genes
MTOR
CYFIP2
TSC2
MAPKBP1
ATRX
PTCH2
PIF1
PIK3CA
KANSL1
MEN1
TP53
MAP4K2
PIK3C2A
DAXX
MAPK9
KISS1
PTEN
SMAD4
KRAS
WNT1
0
100
200
300
N
Intron
Silent
Missense mutation
Nonsense mutation
Splice site
3'UTR
Frame shift insertion
Frame shift deletion
5'UTR
In frame deletion

Possible protein impact

Filtered SNVs
n = 72

Abundance

High abundance SNVs
≥ 10% of reads
n = 42

Low-abundance SNVs
< 10% of reads
n = 30

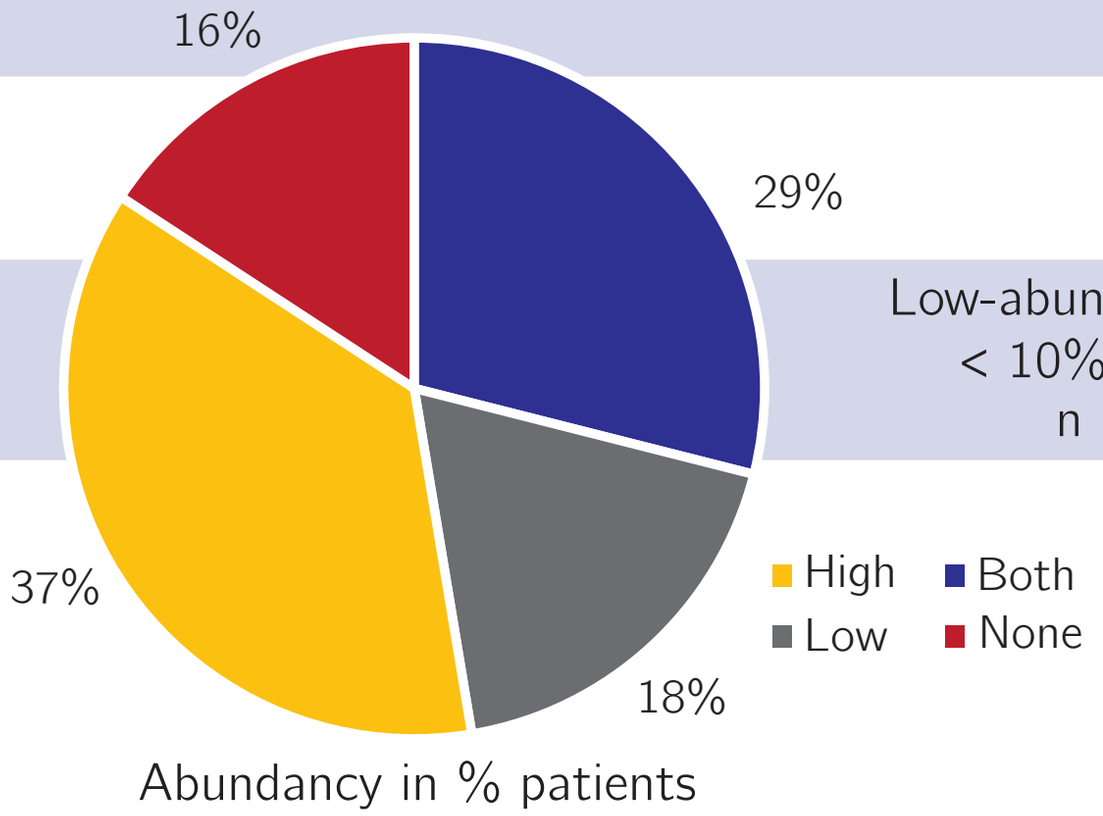

Validation

Somatic
n = 32

Germline
n = 3

Not validated
n = 7

Assumed somatic
n = 30

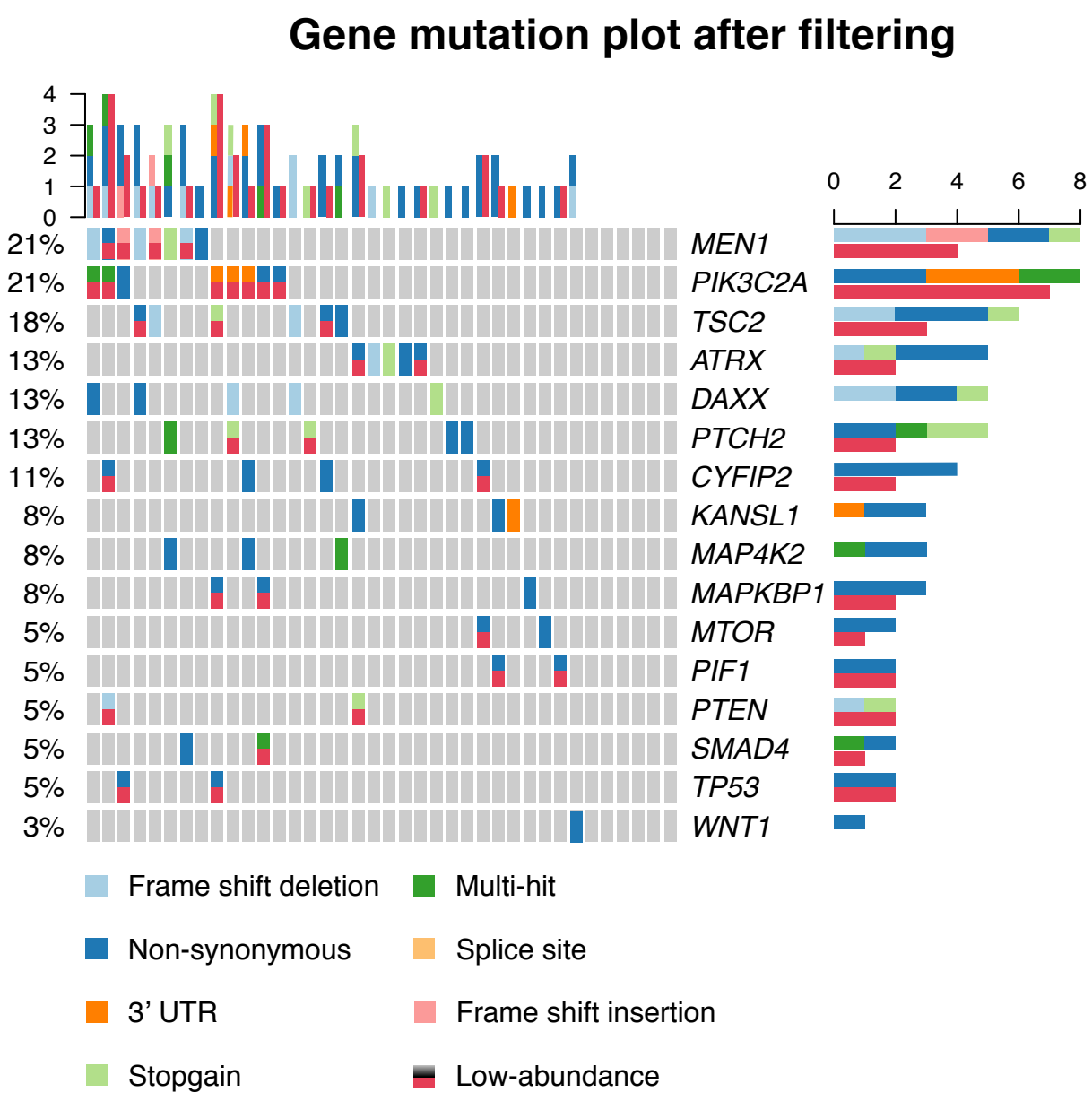
Gene mutation plot after filtering
4
3
2
1
0
0
2
4
6
8
21% MEN1
21% PIK3C2A
18% TSC2
13% ATRX
13% DAXX
13% PTCH2
11% CYFIP2
8% KANSL1
8% MAP4K2
8% MAPKBP1
5% MTOR
5% PIF1
5% PTEN
5% SMAD4
5% TP53
3% WNT1
Frame shift deletion
Multi-hit
Non-synonymous
Splice site
3' UTR
Frame shift insertion
Stopgain
Low-abundance